Am J Physiol Heart Circ Physiol 319: H927–H937, 2020.
First published August 21, 2020; doi:10.1152/ajpheart.00546.2020.

RESEARCH ARTICLE | *Cardiovascular Neurohormonal Regulation*

Functional coculture of sympathetic neurons and cardiomyocytes derived from human-induced pluripotent stem cells

Annika Winbo,[1,2,3] Suganeya Ramanan,[1,2] Emily Eugster,[4] Stefan Jovinge,[4,5] Jonathan R. Skinner,[2,3] and Johanna M. Montgomery[1,2]

[1]*Department of Physiology, The University of Auckland, Auckland, New Zealand;* [2]*Manaaki Mānawa Centre for Heart Research, The University of Auckland, Auckland, New Zealand;* [3]*Department of Paediatric and Congenital Cardiac Services, Starship Children's Hospital, Auckland, New Zealand;* [4]*DeVos Cardiovascular Research Program, Spectrum Health and Van Andel Research Institute, Grand Rapids, Michigan; and* [5]*Cardiovascular Institute, Stanford University, Palo Alto, California*

Submitted 2 July 2020; accepted in final form 20 August 2020

Winbo A, Ramanan S, Eugster E, Jovinge S, Skinner JR, Montgomery JM. Functional coculture of sympathetic neurons and cardiomyocytes derived from human-induced pluripotent stem cells. *Am J Physiol Heart Circ Physiol* 319: H927–H937, 2020. First published August 21, 2020; doi:10.1152/ajpheart.00546.2020.—Sympathetic neurons (SNs) capable of modulating the heart rate of murine cardiomyocytes (CMs) can be differentiated from human stem cells. The electrophysiological properties of human stem cell-derived SNs remain largely uncharacterized, and human neurocardiac cocultures remain to be established. Here, we have adapted previously published differentiation and coculture protocols to develop feeder-free SNs using human-induced pluripotent stem cells (hiPSCs). hiPSC-SNs were characterized in monoculture and coculture with hiPSC-CMs, using antibody labeling, enzyme-linked immunosorbent assay, and whole cell patch-clamp electrophysiology techniques. hiPSC-SNs stained positive for peripherin, tyrosine hydroxylase, and nicotinic acetylcholine receptors, the latter two colocalizing in somas and synaptic varicosities. hiPSC-SNs functionally matured in vitro and exhibited healthy resting membrane potentials (average = -61 ± 0.7 mV), secreted norepinephrine upon activation, and generated synaptic and action currents and inward and outward voltage-dependent currents. All hiPSC-SNs fired action potentials in response to current injection, local application of potassium, or spontaneously, followed by short-medium afterhyperpolarizations. hiPSC-SNs could successfully be maintained in coculture with hiPSC-CMs, and this induced further development of hiPSC-SN action potential kinetics. To test functional coupling between the neurons and cardiomyocytes, the hiPSC-CM beating response to nicotine-induced norepinephrine release was assessed. In neurocardiac cocultures, nicotine exposure significantly increased the hiPSC-CM spontaneous beating rate, but not in hiPSC-CM monocultures, supporting nicotinic neuronal hiPSC-SN stimulation directly influencing hiPSC-CM function. Our data show the development and characterization of electrophysiologically functional hiPSC-SNs capable of modulating the beating rate of hiPSC-CMs in vitro. These human cocultures provide a novel multicellular model to study neurocardiac modulation under physiological and pathological conditions.

NEW & NOTEWORTHY We present data on a functional coculture between human-induced pluripotent stem cell-derived sympathetic neurons and cardiomyocytes. Moreover, this study adds significantly to the available data on the electrophysiological function of human-induced pluripotent stem cell-derived sympathetic neurons.

human-induced pluripotent stem cells; neurocardiac coculture; sympathetic modulation of heart rate; sympathetic neurons

INTRODUCTION

The sympathetic nervous system, responsible for the "fight or flight" response, regulates heart rate and vascular dynamics under a range of physiological conditions (27). During development, migrating neural crest cells form the paravertebral sympathetic chain and segregate into discrete ganglia before differentiating into sympathetic neurons (1, 5). Cardiac-projecting postganglionic sympathetic neurons innervate the myocardium via a network of nerve fibers whose distribution is regulated by the availability of neurotrophic growth factors released from the cardiac tissue during organogenesis (13, 15, 34). Functional neurocardiac coupling is characterized by the presence of sympathetic presynaptic varicosities, closely opposed and specialized pre- and postsynaptic cell membranes, postsynaptic receptors on cardiomyocytes, and neurotransmitter vesicles that release norepinephrine via calcium-dependent exocytosis as a response to activation of nicotinic acetylcholine (ACh) receptors (15, 18, 37).

Sympathetic activity modulates ventricular repolarization, and its dysregulation or hyperactivity contributes to the pathophysiology of both primary and secondary cardiovascular diseases (10, 27, 36, 45). Increased β-adrenergic signaling during emotional or physical stress is an established trigger of life-threatening cardiac events in inherited arrhythmia syndromes such as the long QT syndrome and catecholaminergic polymorphic ventricular tachycardia (40). Neuromodulators (such as β-blockers and cardiac sympathetic denervation) are mainstay preventive therapeutic options for these and other arrhythmias; however, the cellular basis underlying sympathetic triggering of arrhythmia remains incompletely characterized (40, 44).

There are few physiologically relevant tools to model the cellular mechanisms underlying sympathetic (dys)regulation of cardiovascular targets in humans. Animal neurocardiac models have provided important insights into the molecular and physiological underpinnings of autonomic dysregulation and remodeling in cardiac disease (17, 25, 35); however, with regard to inherited arrhythmia syndromes, molecular contributors of cardiac repolarization differ between species (26, 29, 30).

Correspondence: A. Winbo (a.winbo@auckland.ac.nz).

During the past decades, pluripotent stem cells have emerged as an important source of human cells in which cellular development and function can be studied in vitro under physiological and pathophysiological conditions (8, 9, 20, 31, 38, 39). The human cell source used is either embryonic stem cells (heSCs) derived from early preimplantation embryos (43) or induced pluripotent stem cells (hiPSCs), reprogrammed from skin fibroblasts or peripheral blood mononuclear cells, based on derivations of Yamanka's Nobel Prize-winning research (41).

It was shown in 2016 by Oh et al. (32) that human stem cells can be differentiated into norepinephrine-secreting sympathetic neurons, capable of modulating the heart rate of neonatal mouse ventricular cardiomyocytes when cocultured in vitro. However, functional coupling between human stem cell-derived sympathetic neurons and hiPSC-derived cardiomyocytes was not achieved (32). Moreover, a recent study in 2020 by Takayama et al. (42) presented data on sympathetic-like neurons, without measurable norepinephrine secretion, but with moderate effects on the hiPSC-derived cardiomyocyte beating rate. Importantly, the electrophysiological properties of human stem cell-derived sympathetic neurons remain largely uncharacterized, and the functional maturation of stem cell-derived cells, including cardiomyocytes, has increasingly been put into question (24).

Here, we describe the development and functional characterization of sympathetic neurons derived from human-induced pluripotent stem cells (hiPSC-SNs) and their coculture with hiPSC-derived cardiomyocytes (hiPSC-CMs).

METHODS

Ethics. The study has been approved by institutional review committees in Umeå, Sweden (Regional Ethics Committee, Umeå University: Dnr 05-127M), and Auckland, New Zealand (Health and Disability Ethics Committees: 17/NTA/226), and all the participants have provided written informed consent.

Reprogramming of peripheral blood mononuclear cells into hiPSCs. Peripheral blood mononuclear cells from a healthy adult male were reprogrammed using an integration-free kit (CytoTune-iPS 2.0 Sendai Reprogramming Kit, Invitrogen, Life Technologies, now Thermo Fisher, Cat. Nos. A16517 and A16518). Putative hiPSC clones were validated by immunostaining for pluripotency markers SSEA4, Oct4, Tra-1–60, and Sox2. Validated hiPSC clones were expanded on Geltrex-coated 12-well plates in Essential 8 medium, passaged at ~85% confluency using Accutase dissociation enzyme (37°C, <2 min) in the presence of Thiazovivin selective inhibitor of rho-associated kinase, and frozen in Bambanker freezing media, in accordance with previously published protocols (38). The passage number of the frozen hiPSC clones used for this study was between 30 and 35.

Neuronal induction, differentiation, and maturation of sympathetic neurons from hiPSCs. Neuronal differentiation was repeated five or more times to ensure phenotypic consistency over multiple differentiation rounds. The optimized neuronal induction and differentiation protocol (Fig. 1) was based on previously published protocols (8, 9, 32, 39) and modified for feeder-free culture conditions (detailed protocol available at https://doi.org/10.6084/m9.figshare.12756239). In summary, thawed hiPSCs were plated onto Geltrex-coated 12-well plates and cultured in StemFlex medium. Induction (*day 0*) was initiated at 70–80% confluency (9), and over the first 2 wk, a series of small molecules, the majority inhibitors, were added sequentially. From *day 4*, the culture medium was gradually exchanged from StemFlex medium to N2-supplement-enriched B-27 plus neuronal culture system by 25% increments every other day. On *day 12*, the cells were passaged using Accutase dissociation enzyme (37°C, ca. 20–25 min), resuspended in N2 media (concentration = 5×10^6 cells/mL), and replated on Geltrex-coated 12-mm glass coverslips placed in 24-well plates ($1–2 \times 10^6$ precursor cells/well) in neuronal medium and BMP4. From *day 14*, the cells were cultured in neuronal medium (B-27 plus neuronal culture system + 2 mM L-glutamine, N-2 supplements, 0.2 mM ascorbic acid, 0.2 nM dbcAMP, 10 ng/mL NGF, 10 ng/mL BDNF, and 10 ng/mL GDNF) for further neuronal maturation. All cells were maintained at 37°C and 5% CO_2 in a humidified incubator.

Differentiation of cardiomyocytes from hiPSCs. Our optimized cardiomyocyte differentiation protocol is based on a previously published small molecule-modulated differentiation protocol (38). Briefly, thawed hiPSCs were plated on Geltrex-covered 12-well plates (0.3×10^6 cells/well) and cultured in StemFlex medium. On *day 0*, at ~85% confluency, the culture medium was changed to RPMI/B27-insulin medium with 6 μM GSK3-β inhibitor CHIR9902, followed by RPMI/B27-insulin medium with 5 μM Wnt inhibitor IWR1 on *day 3*. From *day 7*, the cells were grown in RPMI/B27+insulin medium, replaced every 72 h.

hiPSC-SN and hiPSC-CM coculture conditions. To generate neurocardiac cocultures, visibly beating areas of hiPSC-CMs (aged ≥21 days after the start of differentiation) were manually dissected from

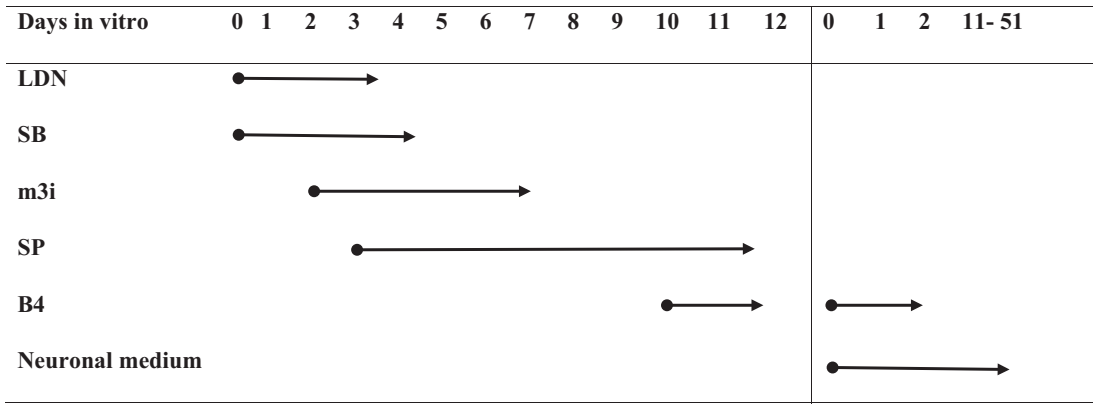

Fig. 1. Overview of small molecule neuronal induction and maturation protocol. LSB = inh LDN 193189 (500 nM) + SB431542 (10 μM) (*days 0–3/4*). m3i = inh CHIR99021 (3 μM) + DAPT (10 μM) + PD173074 (0.2 μM) (*days 2–7*). SP = Shh C25II (50–200 ng/mL) + PMP purmorphamine (1 μM) (*days 3–12*). B4 = BMP4 (10 ng/mL) (*days 10–12 + days 0–2* after replating). Vertical line between *day 12* and *day 0* = dissociation and replating. Neuronal medium = B-27TM Plus Neuronal Culture System + 2 mM L-glutamine, N-2 supplements, 0.2 mM ascorbic acid, 0.2 nM dbcAMP, 10 ng/mL NGF, 10 ng/mL BDNF, and 10 ng/mL GDNF. Adapted protocol based on previously published protocols (8, 9, 32, 39).

their culture wells and dissociated using 1 mg/mL collagenase B (Roche) in RPMI/B27+insulin medium (37°C, 18 h). Dissociated hiPSC-CMs were seeded onto 12-mm glass coverslips coated with Geltrex, containing established mature hiPSC-SNs (≥51 days since pluripotency) (32). One confluent 12-well plate of beating hiPSC-CMs was seeded onto 24 coverslips with mature hiPSC-SNs. The cocultures were maintained in a 50/50 mixture of B-27 plus neuronal culture system and RPMI/B27+insulin medium, replaced every 72 h, for a minimum of 7 days before imaging or electrophysiological characterization.

Immunohistochemistry and imaging. Live cells were visualized under bright-field illumination using an Olympus CKX41 microscope at ×20 magnification. For immunohistochemistry, cells were fixed in 4% paraformaldehyde for 20 min at room temperature, permeabilized in 0.1% TritonX-100/PBS, and labeled with the primary antibodies PHOX2B (1/100, rabbit IgG, Cat. No. ab183741, Abcam), tyrosine hydroxylase (1/500, guinea pig polyclonal anti-serum 2, Cat. No. 213 104, Synaptic Systems), peripherin (1/100, rabbit polyclonal, Cat. No. ab1530, Chemicon), α-bungarotoxin (1/500, pan-nicotinic receptor antagonist, af647, Invitrogen), or troponin T (1/500, mouse monoclonal, Cat. No. MA5-12960, Invitrogen) at 4°C for 20–25 h. After PBS washes, secondary antibodies (Alexa Fluor 488, 568, and 647, Thermo Fisher; 1:500) and Hoechst nuclear stain solution (Sigma-Aldrich) were applied at room temperature for 1 h and 20 min, respectively. Cells were mounted in Citifluor on glass slides, and epifluorescence imaging was performed at ×20–40 magnification using a Zeiss Axioplan 2 fluorescence microscope with a photometrics camera and MetaMorph version 7.8.3 for acquisition, image processing, and analysis (molecular devices). Exposure times were optimized per antibody and were kept consistent across all image acquisitions. Images were generated in ImageJ. Immunostaining per nucleated cell count (Marker$^+$/DAPI$^+$) and colocalization of staining within soma

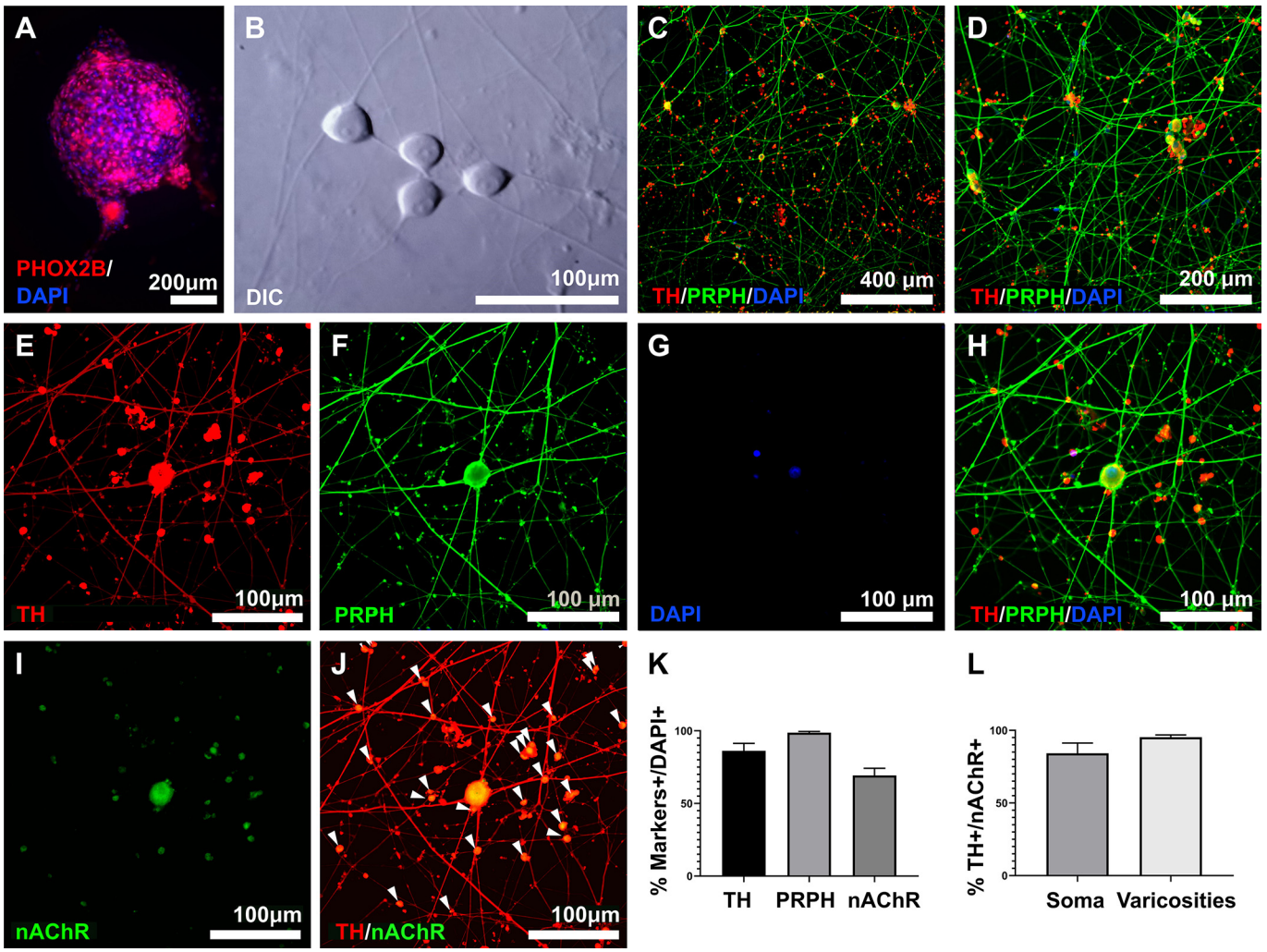

Fig. 2. Cellular morphology and immunohistochemistry staining support a sympathetic neuronal fate of human-induced pluripotent stem cell-derived sympathetic neurons (hiPSC-SNs). *A*: immunohistochemistry staining of a *day 26* neurosphere, positive for the neural crest marker PHOX2B (red) and DAPI (blue) (×10). Scale bar = 200 µm. *B*: *day 83* hiPSC-SNs, visualized under ×40 magnification infrared-differential interference contrast optics, show the typical sympathetic neuronal "beads on a string" growth morphology. Scale bar = 100 µm. *C–J*: immunohistochemical staining of *day 54* hiPSC-SNs, positive for the sympathetic neuronal enzyme tyrosine hydroxylase (TH, red) and peripheral neuronal marker peripherin (PRPH, green). hiPSC-SNs display characteristic punctate TH staining of the varicosities, indicative of sites of synapse formation (*C, D,* and *E*). Nicotinic acetylcholine receptor (nAChR, green) antagonist α-bungarotoxin labeling of the primary synaptic receptor in post-ganglionic sympathetic neurons, consistently colocalized with TH immunostaining in the somas and in the synaptic varicosities of TH-positive cells (*J*). *C*: ×10. *D*: ×20. *E–J*: same image (×40). *H*: image overlay with colocalized TH/PRPH staining appearing yellow. *J*: image overlay with colocalized TH/nAChR staining appearing yellow (white arrowheads). Scale bar = 100 µm. *K*: quantification of TH-, PRPH-, and nAChR-positive cells (DAPI+ n = 161, 11 images). *L*: quantification of TH/nAChR colocalization in nAChR-positive soma and varicosities (nAChR+ puncta n = 869, 15 images). Scale bar = 400 µm (*C*), 200 µm (*D*), and 100 µm (*E, F, G, H,* and *I*). Error bars represent standard error mean.

and varicosities ($TH^+/nAChR^+$) were analyzed in 10–15 images generated from multiple independent culture preparations at ×40 magnification and presented as average percentages ± SE.

Measurement of norepinephrine concentrations in tissue culture medium. An enzyme-linked immunosorbent assay was used to measure norepinephrine release following stimulation with 50 mM KCl, according to the manufacturer's instruction (Aviva Systems Biology Noradrenaline ELISA Kit; OKEH02565).

Whole cell electrophysiology recordings of hiPSC-SNs and hiPSC-CMs. Whole cell patch-clamp recordings were performed at room temperature on hiPSC-SN monocultures and at 37°C on hiPSC-CM monocultures and hiPSC-SN/hiPSC-CM cocultures, grown on 12-mm Geltrex-covered glass coverslips. Cells were visualized under infrared-differential interference contrast optics (ORCA R2, Hamamatsu) at ×40 magnification. hiPSC-SN coverslips were perfused with extracellular solution containing (in mM) 119 NaCl, 2.5 KCl, 2.5 $CaCl_2$, 1 Na_2HPO_4, 1.3 $MgSO_4$, 26.2 $NaHCO_3$, and 11 D-(+)-glucose, adjusted to pH 7.4 with NaOH. hiPSC-SN internal solution consisted of (in mM) 120 K gluconate, 40 HEPES, 5 $MgCl_2$, 2 Na-ATP, and 0.3 Na-GTP, pH adjusted to 7.2 with KOH. For hiPSC-CM whole cell patch-clamp experiments, previously published hiPSC-CM internal and external solutions were used (31). Whole cell patch-clamp recordings were acquired with a MultiClamp 700B amplifier, low-pass filtered at 10 kHz, without leak subtraction, and analyzed using pCLAMP 10.2 software. Recordings with an access resistance exceeding 20 MΩ were discarded.

To characterize active and passive membrane properties, the resting membrane potential (mV), cell capacitance (pF), and action potential kinetics for each hiPSC-SN were recorded. To capture spontaneous hiPSC-SN synaptic current activity, cells were voltage-clamped close to resting membrane potential (−70 mV) and 5-min gap-free recordings were performed. Total current-voltage (*I-V*) relations were determined by 10-mV incremental voltage steps from −80 to +70 mV, with a duration of 1,000 ms per step, and presented normalized to the cell membrane capacitance to obtain total peak current density voltage curves [(pA/pF)/mV] (11, 19, 32).

Spontaneous hiPSC-SN action potential frequency was assessed via 5-min gap-free recordings in current clamp. Action potential firing in response to locally applied 120 mM potassium solution was assessed in a subset of cells. The hiPSC-derived neurons' propensity to fire action potentials upon current injection was characterized by 100-pA incremental current steps of 100–800 pA, with a duration of 200 ms per step. Action potential properties [peak amplitude (mV), maximum rise slope (pA/ms), rise time (ms), decay time (ms), action potential duration half-width (APD_{50}, ms), and action potential duration at 90% (APD_{90}, ms)] were measured in the first action potential elicited by current injection (100–300 pA, 200-ms duration). The afterhyperpolarization (AHP) duration, i.e., from the time point where

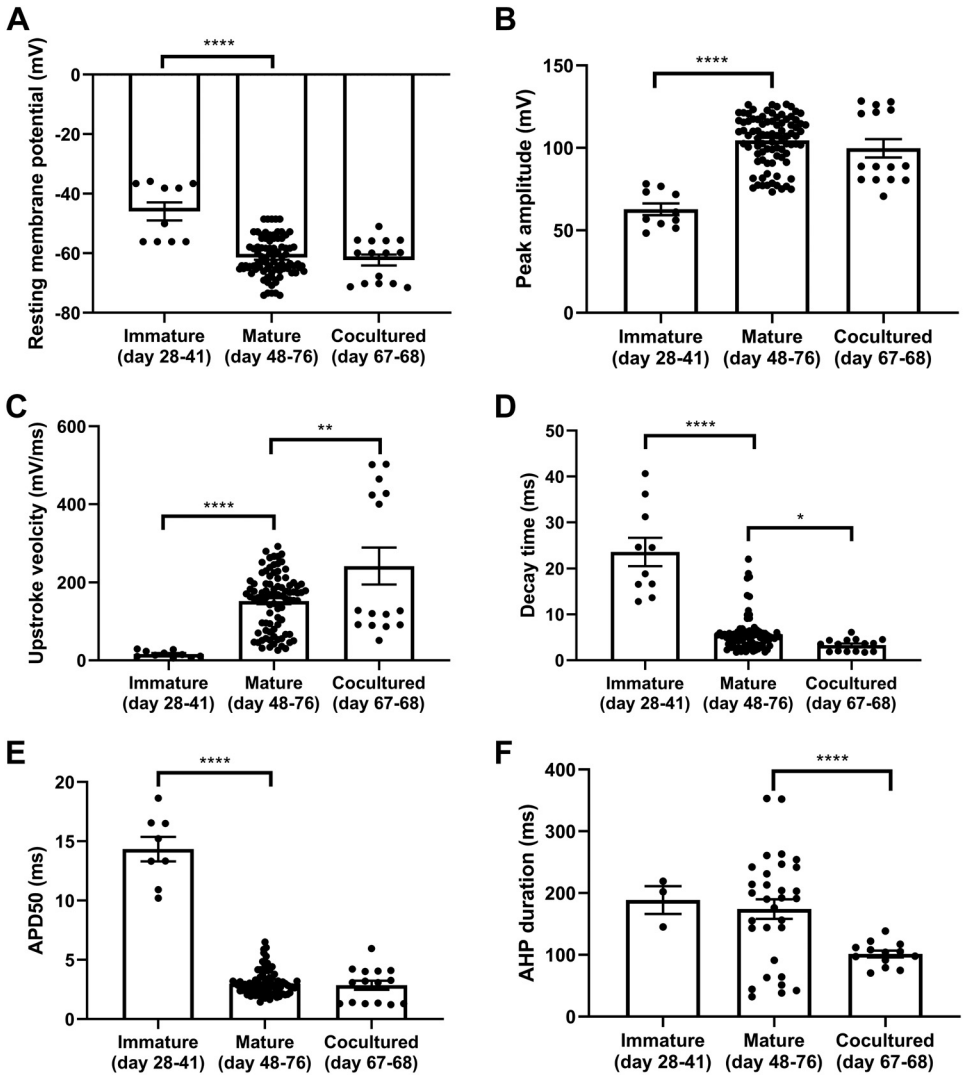

Fig. 3. Membrane and action potential characteristics as stratified by maturation time and coculture conditions. Data were compiled from experiments performed in cultures from five separate differentiation rounds. Comparison across human-induced pluripotent stem cell-derived sympathetic neurons (hiPSC-SNs) for 28–41 days in monoculture ($n = 10$), 48–76 days in monoculture ($n = 87$), and hiPSC-SNs for 67–68 days, including 14 days in hiPSC-SN/human-induced pluripotent stem cell-derived cardiomyocytes coculture ($n = 15$). *A–E*: a significant maturation was seen across action potential characteristics from *days 28–41* to *days 48–76* in monocultured hiPSC-SNs ($P < 0.0001$, *A–E*). After 14 days in coculture, faster action potential kinetics were noted in cocultured hiPSC-SNs compared with mature hiPSC-SNs kept in monoculture with regard to increase in max upstroke velocity (242 ± 47 vs. 152 ± 8 mV/ms, $P = 0.001$) (*C*), decrease in decay time (3.3 ± 0.3 vs. 5.7 ± 0.4, $P = 0.02$) (*D*), and shortening of AHP duration (101 ± 5 ms vs. 174 ± 16 ms, $P = 0.006$) (*F*). All graphs are presented as means ± SE. AHP, afterhyperpolarization; APD_{50}, action potential duration at 50% repolarization. *$P < 0.05$, **$P < 0.01$, and ****$P < 0.0001$.

the action potential passes the resting membrane potential on its decaying slope to when it returns to baseline (in ms), and the AHP amplitude, i.e., from the baseline resting membrane potential to the most hyperpolarized potential reached (in mV), were measured in spontaneously firing hiPSC-SNs with up to five consecutive AHPs analyzed per cell.

Assessment of functional coupling in neurocardiac cocultures. In the established hiPSC-SN and hiPSC-CM cocultures, video analysis of cardiomyocyte beating rate changes triggered by sympathetic stimulation was performed. Coculture coverslips were transferred to a recording chamber, perfused with extracellular solution at 37°C (31), and habituated for a minimum of 10 min before capture. Beating cardiomyocyte syncytia visibly connected to sympathetic neurons were visualized under IR-DIC optics (ORCA-R2, Hamamatsu) at ×40 magnification, with 5-min live capture installments of beating rate during baseline, wash-in, and exposure to 1 μM nicotine to specifically stimulate sympathetic neurons to release norepinephrine (32). This experiment was repeated in hiPSC-CM monocultures, as a negative control.

Statistical analysis. Differences between groups were assessed using analysis of variance, unpaired t test, or χ^2 test, depending on the included variables. For all analyses, a two-tailed value of $P < 0.05$ was considered statistically significant. Continuous variables are presented as means ± SE, and dichotomous variables are presented as n (%).

RESULTS

Morphological and immunohistochemical characterization of hiPSC-SNs in monoculture. During the first week of maturation after neuronal induction, progressive neurite outgrowth was observed in attached cells, as well as formation of neuro-

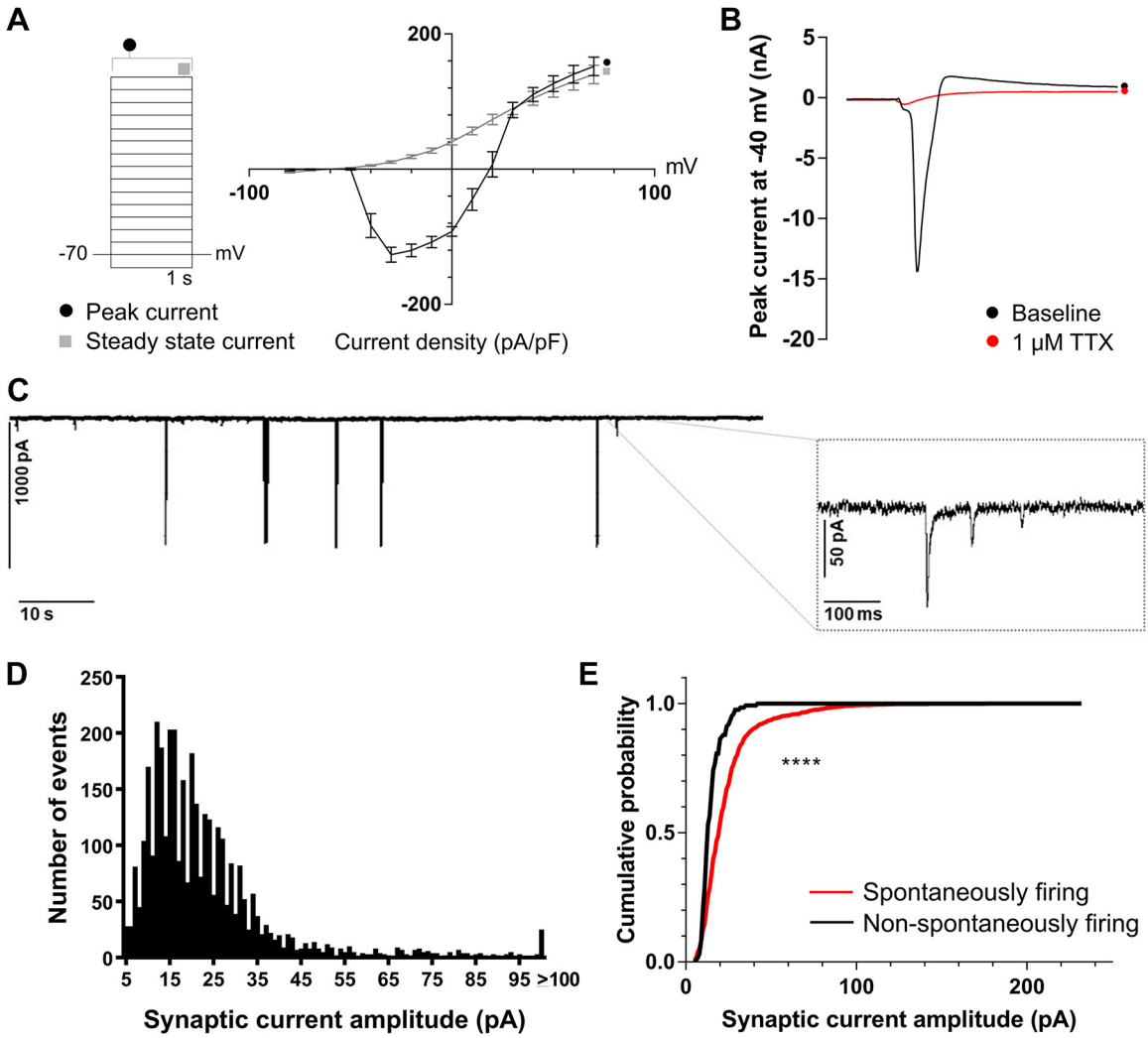

Fig. 4. Whole cell patch-clamp recordings from human-induced pluripotent stem cell-derived sympathetic neurons (hiPSC-SNs) verify the presence of voltage-gated channels generating substantial inward and outward currents, and frequent synaptic activity. Data were compiled from experiments performed in cultures from five separate differentiation rounds. *A*: voltage step protocol (10 mV incremental steps from −80 to +70 mV) and total whole cell current, corresponding to peak and steady-state currents, was measured in *day 48–76* for hiPSC-SNs ($n = 24$). The current density (pA/pF)–voltage (mV) relationships were obtained by normalizing the total currents (pA) to the cell capacitance (pF), and subsequently averaged over all cells (error bars represent standard error mean). *B*: representative peak current trace (duration 30 ms) on *day 53* for hiPSC-SN at −40 mV (black), amplitude −14 nA. The inward current was abolished by 1 μM tetrodotoxin (red). *C*: representative trace depicting spontaneous current activity at −70 mV, with inward (unclamped) action currents, and frequent synaptic currents (shown in magnification, right). *D*: histogram depicting the distribution of synaptic current amplitudes across all spontaneous current recordings in 22 hiPSC-SNs (mean 24 ± 0.3 pA). *E*: cumulative probability plot depicting synaptic current amplitudes for spontaneously firing hiPSC-SNs (red, $n = 19$, 3,425 synaptic currents) and hiPSC-SNs where action potential induction required current injection (black, $n = 3$, 121 synaptic currents). Mean synaptic current amplitude was significantly larger in spontaneously firing hiPSC-SNs compared with nonfiring hiPSC-SNs, 24 ± 0.3 pA versus 15 ± 0.5 pA, ****$P < 0.0001$.

spheres staining positive for neural crest marker PHOX2B, a key transcription factor for sympathetic neuronal development (Fig. 2*A*). Mature hiPSC-SNs showed morphological features of sympathetic neuronal differentiation, including establishment of extensive processes and the characteristic "shiny beads on a string" phenotype (Fig. 2*B*). hiPSC-SNs were positive for the rate-limiting enzyme in catecholamine synthesis tyrosine hydroxylase (TH, 86% of nucleated cells) and for peripherin, an intermediate filament expressed in neurons of the peripheral nervous system (PRPH, 99% of nucleated cells), both staining the soma and processes of the hiPSC-SNs (Fig. 2, *C–H*). Notably, hiPSC-SNs displayed characteristic punctate TH staining in the varicosities of the neuronal processes, indicative of synaptic sites (Fig. 2, *C–E*) (7, 15). Ionotropic nicotinic acetylcholine receptors (nAChRs) were present in the hiPSC-SNs, as evident by punctate staining with α-bungarotoxin, an nAChR antagonist, known from animal studies to stain postganglionic neurons and synaptic densities in sympathetic ganglia (Fig. 2, *I* and *J*) (37). The nAChR staining colocalized with TH staining in the soma (84% of nAChR-positive somas) and synaptic varicosities of the hiPSC-SNs (95% of nAChR-positive puncta outside of the soma, Fig. 2*J*, white arrowheads, with quantification in Fig. 2, *K* and *L*).

Characterization of hiPSC-SN physiological maturation in monoculture. We examined the electrophysiological characteristics of hiPSC-SNs throughout different periods in monoculture. We noted significant electrophysiological maturation over time in the hiPSC-SNs, from an immature electrophysiological phenotype in *day 28–41* hiPSC-SNs ($n = 10$) to a mature phenotype in *day 48–76* hiPSC-SNs ($n = 87$, Fig. 3). Specifically, increased time in culture from 28–41 days to 48–76 days significantly hyperpolarized the resting membrane potential (from -46 ± 5 to -61 ± 0.7 mV). Moreover, increased time in culture increased the peak action potential amplitude,

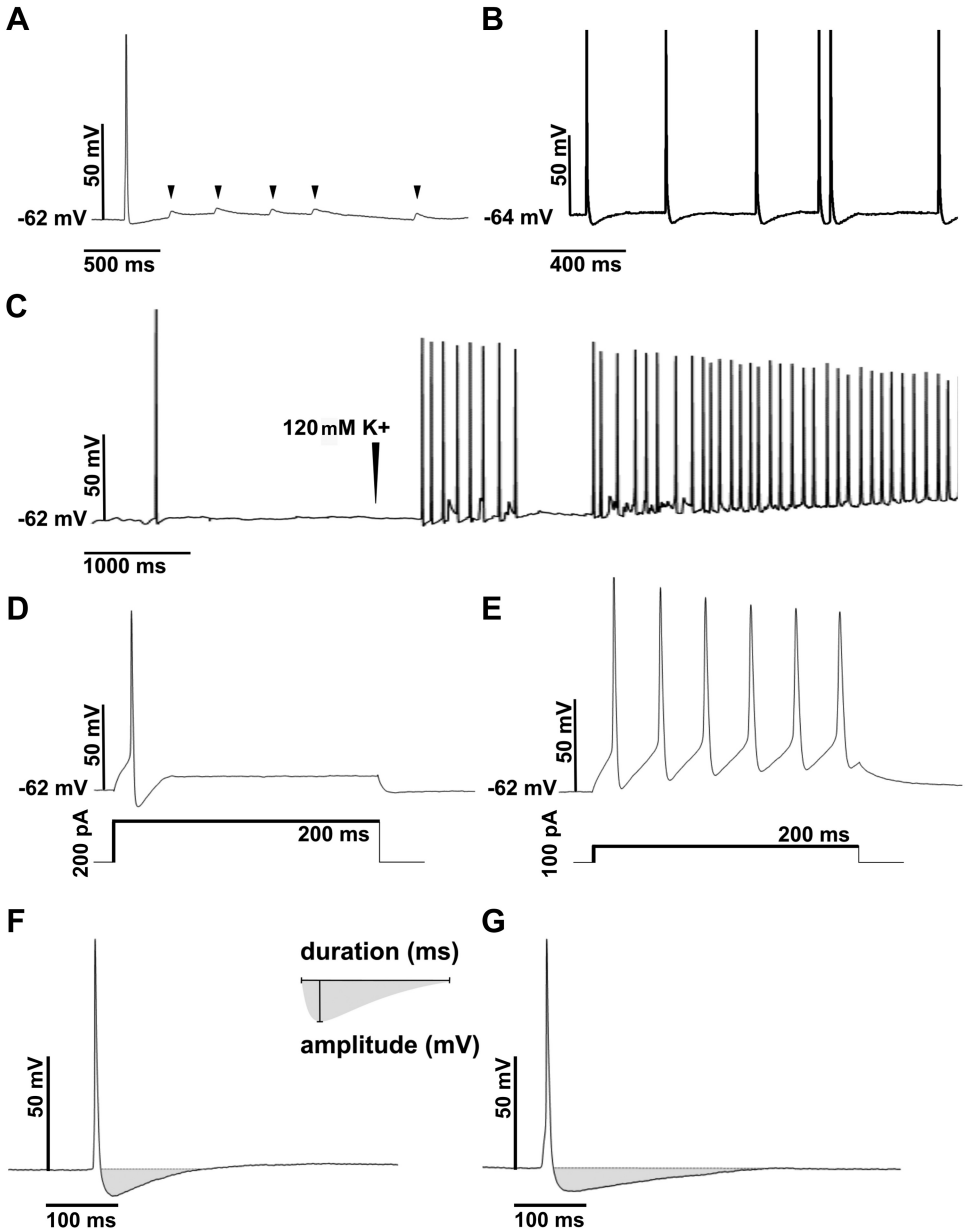

Fig. 5. Representative examples of action potentials in human-induced pluripotent stem cell-derived sympathetic neurons (hiPSC-SNs). Data were compiled from experiments performed in cultures from five separate differentiation rounds. *A–C*: spontaneous action potential firing, single (*A*) or multiple (*B*), was noted on *days 53–59* for hiPSC-SNs during gap-free 5-min current clamp recordings ($n = 21$ cells). In the same cells, excitatory postsynaptic potentials were frequently seen (*A*, arrowheads). *C*: spontaneously firing hiPSC-SN, exposed to 120 mM potassium (arrowhead), responded with multiple rapid action potentials and subsequent membrane depolarization (9/9 exposed cells responded similarly). *D–E*: action potentials (single or multiple) could be evoked in all hiPSC-SNs by 100–300 pA current injection ($n = 30$). *D*: example phasic response to a current injection of 200 pA, duration 200 ms [single-action potential, seen in 8/30 (27%) of hiPSC-SNs]. *E*: example tonic response to a current injection of 100 pA, duration 200 ms [multiple action potentials, seen in 22/30 (73%) of hiPSC-SNs]. *F–G*: representative examples of short (117 ± 11 ms, -8.6 ± 1.2 mV, 22/36, *F*) and medium (330 ± 20 ms, -9.8 ± 1.0 mV, 14/36, *G*) afterhyperpolarizations.

Table 1. *Action potential firing characteristics for hiPSC-SNs after 100–300 pA current injection*

	$n = 30$
Mean age, days after hiPSC stage ± SE	59 ± 1.4
Resting membrane potential, mV ± SE	−60 ± 1.9
Membrane capacitance, pF ± SE	85 ± 5.1
Firing spontaneously, *n* (%)	12 (40)
Firing at 100 pA current injection, *n* (%)	16 (53)
First firing at 200 pA, *n* (%)	10 (33)
First firing at 300 pA, *n* (%)	4 (13)
Single (phasic) action-potential firing, *n* (%)	8 (27)
Multiple (tonic) action-potential firing, *n* (%)	22 (73)
Action-potential amplitude, mV ± SE	93 ± 3.9
Max upstroke velocity, pV/ms ± SE	150 ± 16
Rise time, ms ± SE	5.1 ± 0.5
Decay time 90%, ms ± SE	4.1 ± 0.3
Action potential half-width, ms ± SE	2.8 ± 0.2
Action-potential duration 90%, ms ± SE	9.2 ± 0.6

hiPSC, human-induced pluripotent stem cell; hiPSC-SNs, human-induced pluripotent stem cell-derived sympathetic neurons.

increased upstroke velocity, decreased the action potential decay time, and decreased the action potential duration half-time (all $P < 0.0001$, Fig. 3), consistent with faster action potential kinetics of mature neurons.

Functional characterization of mature hiPSC-SNs in monoculture. To verify that activation of hiPSC-SN-induced presynaptic release of norepinephrine, we measured the concentration of norepinephrine in the tissue culture medium of mature neurons, averaging 75 days in culture, using an enzyme-linked immunosorbent assay. As expected, no release was detected at baseline; however, in response to 50 mM KCl, the amount of norepinephrine detected to be released from stimulated hiPSC-SNs was 6.2 ± 2.6 pg/mL ($n = 3$).

To characterize mature hiPSC-SN electrophysiological properties, we performed whole cell patch-clamp experiments. *Day 48–76* hiPSC-SNs ($n = 87$) showed healthy resting membrane potentials, averaging −61 ± 0.7 mV. In voltage-clamp, hiPSC-SNs exhibited functional voltage-gated channels, generating substantial inward and outward currents in response to a voltage step protocol ($n = 24$, Fig. 4*A*). Peak and steady-state currents were measured across the holding potential range of −80 to +70 mV and standardized to the cell capacitance to generate current densities (pA/pF). The total peak current density-voltage relationship, similar to previously published data from 7 heSC-SNs (32), showed that hiPSC-SNs exhibited inward current from −50 mV that reached maximum at −30 mV (−127 ± 11 pA/pF), which reversed at +19 mV to an outward current with a maximum of +152 ± 14 pA/pF at +70 mV. The inward current was blocked by 1 μM tetrodotoxin, supporting that voltage-gated sodium channels contribute to the inward current in hiPSC-SNs (Fig. 4*B*).

During gap-free voltage-clamp recordings where the hiPSC-SN membrane potential was held at −70 mV, spontaneous inward currents were frequently noted ($n = 22$, Fig. 4, *C* and *D*). The spontaneous current activity included action currents (19/22 hiPSC-SNs, amplitude = 2,082 ± 93 pA, frequency = 0.1 ± 0.1 Hz) and synaptic currents (22/22 hiPSC-SNs, amplitude = 24 ± 0.3 pA, frequency = 1.1 ± 0.4 Hz). Synaptic current amplitude was significantly higher in spontaneously firing hiPSC-SNs, as compared with hiPSC-SNs, where action potentials were only inducible by current injection ($P < 0.0001$, Fig. 4*E*).

The hiPSC-SNs' abilities to fire action potentials, either spontaneously or after a triggering stimulus, were assessed in current-clamp mode. All hiPSC-SNs, aged 48–76 days since pluripotency, fired single or multiple action potentials either spontaneously ($n = 21$, Fig. 5, *A* and *B*), following local exposure to 120 mM potassium ($n = 9$, Fig. 5*C*), or upon current injection (100–300 pA; $n = 30$, Fig. 5, *D* and *E*). In gap-free recordings of spontaneously firing hiPSC-SNs ($n = 21$), excitatory postsynaptic potentials (EPSPs) were frequently noted (Fig. 5*A*, arrowheads).

The characteristics of hiPSC-SN action potential firing induced by current injection (100–300 pA, 200-ms duration) are summarized in Table 1 ($n = 30$). The hiPSC-SNs responded with either a phasic (single action potential, 27% of cells, Fig. 5*D*) or tonic firing pattern (multiple action potentials, 73% of cells, Fig. 5*E*).

Afterhyperpolarization (AHP) duration and amplitude were measured in 12 spontaneously firing hiPSC-SNs (Table 2). All measured AHPs ($n = 36$) were of either short duration (117 ± 11 ms, −8.6 ± 1.2 mV, 22/36, Fig. 5*F*) or medium duration (330 ± 20 ms, −9.8 ± 1.0 mV, 14/36, Fig. 5*G*).

Establishment of functionally coupled neurocardiac cocultures. As well as characterizing hiPSC-SNs in isolation, we successfully cocultured hiPSC-SNs with hiPSC-CMs, to generate a novel human neurocardiac in vitro model (Fig. 6). We were able to maintain neurocardiac cocultures for over 15 days in vitro. Coculture of hiPSC-CM/hiPSC-SN for 14 days further enhanced cocultured hiPSC-SNs' ($n = 15$) action potential kinetics, including increased upstroke velocity (242 ± 47 mV/ms vs. 152 ± 8 pA/ms, $P = 0.001$) and decreased decay time (3.3 ± 0.3 vs. 5.7 ± 0.4 ms, $P = 0.02$), as compared with mature hiPSC-SNs kept in monoculture (Fig. 3, *C* and *D*). Moreover, after 14 days in coculture, the AHPs of the hiPSC-SNs were shortened as compared with mature hiPSC-SNs in monoculture (101 ± 5 ms, $n = 13$ vs. 220 ± 20 ms, $n = 36$).

Qualitative observation of the cocultures showed neurite outgrowth from hiPSC-SNs into troponin T-positive hiPSC-CM clusters (Fig. 6*A*). We observed elongated extension of processes from hiPSC-SNs reaching directly into hiPSC-derived cardiomyocyte clusters, with neurites coursing over and through cardiomyocyte syncytia (Fig. 6*B*). Punctate staining of varicosities suggested synaptic connections between the hiPSC-SNs and the hiPSC-CMs (Fig. 6*B*, *inset*).

Table 2. *AHP characteristics for spontaneously firing (hiPSC-SNs) in monoculture*

	All	Short AHP (<221 ms)	Medium AHP (221–428 ms)
n hiPSC-SNs (AHPs)	12 (36)	9* (22)	5* (14)
Mean age, days after hiPSC stage ± SE	62 ± 1.9	60 ± 2.0	65 ± 3.6
Membrane capacitance, pF ± SE	94 ± 6.5	103 ± 9.7	80 ± 5.6
Resting membrane potential, mV ± SE	−58 ± 3.1	−60 ± 0.9	−54 ± 7.9
AHP amplitude, mV ± SE	−9.1 ± 0.8	−8.6 ± 1.2	−9.8 ± 1.0
AHP duration, ms ± SE	220 ± 20	117 ± 11	330 ± 20

AHP, afterhyperpolarization; hiPSC, human-induced pluripotent stem cell; hiPSC-SNs, human-induced pluripotent stem cell-derived sympathetic neurons. *2/12 hiPSC-SNs fired action potentials with both short and medium AHPs.

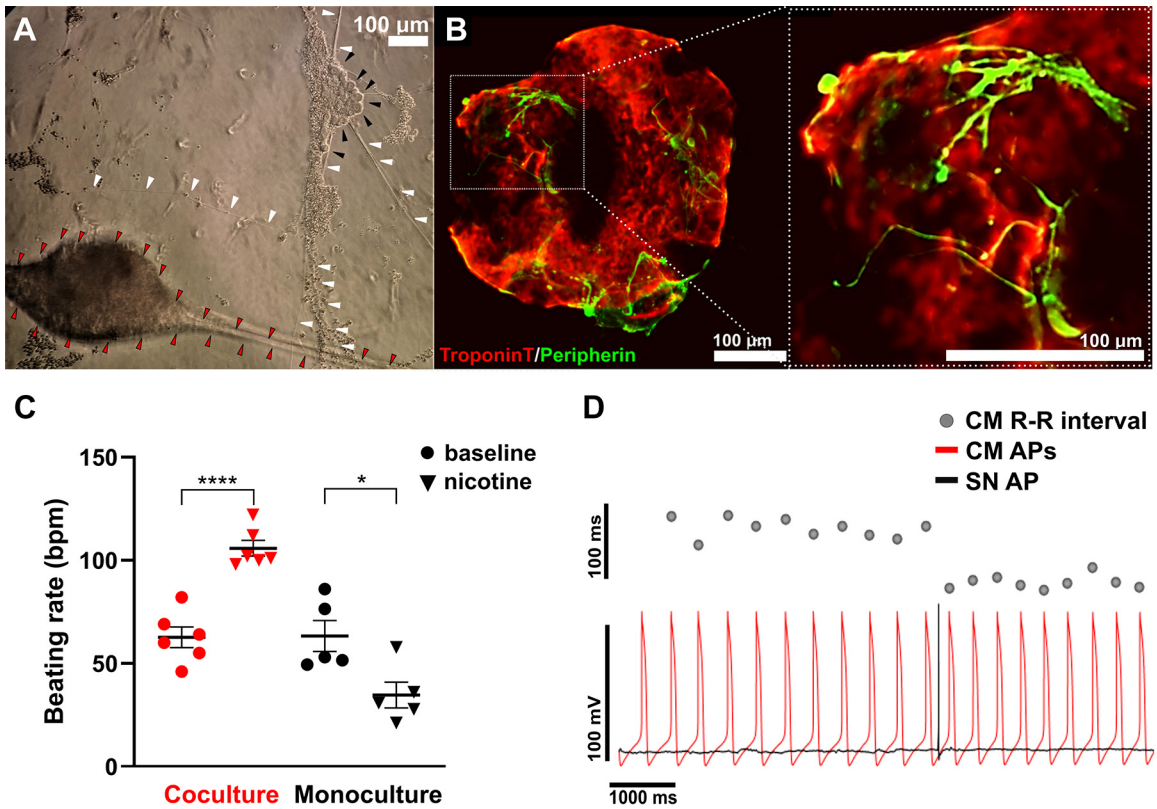

Fig. 6. Coculture and functional connections between human-induced pluripotent stem cell-derived sympathetic neurons (hiPSC-SNs) and human-induced pluripotent stem cell-derived cardiomyocytes (hiPSC-CMs). *A*: beating cardiomyocyte syncytcia (red arrowheads) and cluster of sympathetic neurons (black arrowheads) connected by long neurites (white arrowheads), visualized under ×10 magnification infrared-differential interference contrast optics. *B*: immunohistochemistry staining of cardiomyocyte syncytia (troponin T, red) with hiPSC-SN neurites coursing over and through (immunolabeled for peripherin, green). Punctate staining of varicosities suggests synaptic connections between the hiPSC-SNs and the hiPSC-CMs (*inset* and *right*). *C*: in the neurocardiac cocultures, 1 μM nicotine significantly increased the hiPSC-CM beating rate from 63 ± 5.0 to 106 ± 3.8 beats/min ($P < 0.0001$, $n = 6$) and caused a beating rate decrease in hiPSC-CM monocultures (63 ± 7.5 to 35 ± 6.2 beats/min, $P = 0.02$, $n = 5$). *D*: example of increased hiPSC-CM beating rate (red line, and *top* R-R interval as dots) observed following a hiPSC-SN action potential (black line) during paired simultaneous recording. *$P < 0.05$ and ****$P < 0.0001$.

To determine whether the hiPSC-SNs were forming functional connections with the hiPSC-CMs and could therefore modulate their activity, we added 1 μM nicotine to the recording chamber to stimulate sympathetic neurons to release norepinephrine and then examined whether there was any response in the hiPSC-CMs as measured by change in the beating rate. We quantified the beating rate response to nicotine-induced norepinephrine release in neurocardiac cocultures and repeated the experiment in hiPSC-CM monocultures, as a negative control. In coculture, 1 μM nicotine significantly increased the hiPSC-CM spontaneous beating rate from 63 ± 5.0 to 106 ± 3.8 beats/min ($P < 0.0001$, $n = 6$, Fig. 6*C*, *left*). In contrast, in hiPSC-CM monocultures, 1 μM nicotine decreased the beating rate from 63 ± 7.5 to 35 ± 6.2 beats/min ($P = 0.02$, $n = 5$, Fig. 6*C*, *right*). Moreover, using simultaneous paired recording, an example of increased hiPSC-CM beating rate observed directly following a hiPSC-SN action potential can be seen in Fig. 6*D*.

DISCUSSION

Here, we describe the differentiation of hiPSCs into norepinephrine-secreting cells with morphological, immunohistochemical, and functional electrophysiological properties supporting a sympathetic neuronal fate of the derived cells (hiPSC-SNs). Importantly, the hiPSC-SNs were able to modulate the beating rate of cocultured hiPSC-derived cardiomyocytes (hiPSC-CMs). We also present data supporting that time in monoculture and coculture improves hiPSC-SN maturation.

Implications for generation of physiologically mature hiPSC-SNs. The main data presented in this paper were derived from monocultured hiPSC-SNs matured to *days 48–76*, with a resting membrane potential of −61 ± 0.7 mV ($n = 87$) and with documented action potential firing and synaptic activity. Although Oh et al. (32) performed functional electrophysiological characterization in *day 28* heSC-SNs ($n = 10$) developed from a FACS-sorted PHOX2B::GFP$^+$ reporter line, our experience was that a longer maturation time was needed to establish a mature electrophysiological phenotype in the hiPSC-SNs. This was evident by a significant decrease in resting membrane potential, increase in peak amplitude of action potentials, and improvement of action potential kinetics over the maturation time of the hiPSC-SNs. Indeed, the *day 28* heSC-SNs were more comparable with our immature hiPSC-SNs, with the heSC-SNs' relatively depolarized resting membrane potential [−46 ± 3 mV ($n = 10$), as compared with −46 ± 5 mV in the *day 28–41* hiPSC-SNs ($n = 10$)] and broad action potentials, indicating slow kinetics (32).

In addition, we observed that the AHP duration was shorter in our hiPSC-SNs (hiPSC-SNs: 220 ± 20 ms, $n = 36$; heSC-

SNs: 291 ± 56 ms, $n = 3$), not surprisingly, as AHP decreases with resting membrane hyperpolarization (22). The hiPSC-SNs' AHP duration and amplitude measured in our study were comparable with those of mammalian cervical and thoracic postganglionic sympathetic neurons (with the fusion of the lower cervical and the upper thoracic forming the stellate ganglia that projects to the heart), and none displayed the long AHPs typical for celiac sympathetic ganglia neurons (2, 22, 23).

Moreover, after 14 days in coculture, while remaining at a comparable resting membrane potential, the action potential kinetics of mature hiPSC-SNs significantly improved, and AHP shortened, as compared with that of age-matched hiPSC-SNs kept in monoculture. Although this has not been studied in human-derived cells using electrophysiological techniques before, functional connections with target tissues are known to promote neuronal maturation (4, 14), where expression levels of norepinephrine, nAChRs and sodium and potassium channels were significantly increased in heSC-SNs cocultured with neonatal mouse ventricular myocytes (32).

Nicotine-induced norepinephrine release and neurocardiac coupling. Postganglionic sympathetic neurons express nAChRs and release norepinephrine in response to agonist application (i.e., ACh or nicotine) (37). Importantly, our data show that our human-derived sympathetic neurons express nAChRs on the soma and at putative synaptic varicosities. In coculture, nicotine exposure precipitated an increase in the hiPSC-CM beating rate, suggesting depolarizing activity induced by activation of nicotinic ACh receptors on hiPSC-SNs. The discrete α-bungarotoxin-positive puncta colocalized in TH-positive somas and synaptic varicosities in hiPSC-SNs support the presence of postsynaptically localized α7-nAChRs on postganglionic hiPSC-SNs mediating this effect of nicotine.

In contrast, in hiPSC-CM monocultures, nicotine exposure was associated with a significant beating rate decrease. This finding is likely due to the dual response to activation of nAChR subtypes that are present in cardiomyocytes, i.e., an initial brief bradycardic response followed by a larger and persistent beating rate increase, in the presence of norepinephrine (21). In the absence of sympathetic neurons, however, the slowing of the beating rate persisted throughout the nicotine exposure. The slowing of the hiPSC-CM beating rate in the absence of sympathetic neurons supports that the increased beating rate seen in the neurocardiac cocultures was mediated by hiPSC-SN nicotine-induced norepinephrine release.

Further characterization of the neurocardiac coculture model, including in-depth characterization using paired simultaneous recordings, will be of importance to elucidate mechanisms underlying sympathetic modulation of cardiac function and arrhythmia susceptibility. It is critical to point out that determining the sympathetic neuronal contribution to sympathetic cardiovascular disorders requires the examination of sympathetic neuron-cardiomyocyte interactions rather than assessing responses to sympathomimetics in cardiomyocyte monoculture. As an example, using a neurocardiac coculture model, a dominant role for sympathetic neurons in driving the cardiac phenotype in prohypertensive rats was revealed (28). Moreover, models including not only sympathetic but also parasympathetic neurons would be ideal (42). Neurocardiac modeling in human cells will be key to examining neuronal regulation of cardiac function and deciphering the potential sympathetic neuronal contribution to inherited cardiac disease.

Rationale and implications for our adapted feeder-free protocol. We have established a feeder-free protocol to produce SN cultures and neurocardiac cocultures from hiPSCs without prior gene editing or cell sorting. There are potential advantages to using hiPSCs as a cell source, compared with heSCs, as hiPSCs can be obtained from consenting patients and controls and are associated with less ethical and legal considerations (3). If used for therapeutic implementations, feeder-free culture conditions prevent transfer of animal pathogens that could induce an immune response (16). Our methods enable complete feeder-free generation of patient-derived human neurocardiac cocultures for disease modeling and future translational implementations. As the sympathetic nervous system is an important therapeutic target for antiarrhythmia therapies, including β-blockers and neuromodulatory interventions (6, 12, 33), this coculture model could enable studies into neurocardiac regulatory mechanisms, contributors to arrhythmia, and novel neurocardiac treatment strategies.

Conclusions. We have established novel human neurocardiac cocultures with norepinephrine-secreting and electrophysiologically functional hiPSC-derived sympathetic neurons capable of modulating the beating rate of hiPSC-derived cardiomyocytes. These cocultures could be used to study neurocardiac modulation under normal and pathological conditions, including sympathetically triggered arrhythmias.

GRANTS

This work was funded by Hugh Green Foundation, Cure Kids, and the Auckland Medical Research Foundation (to A. Winbo), and Cure Kids provides salary support (to J. R. Skinner).

DISCLAIMERS

All authors approved the final version of the manuscript and agreed to be accountable for all aspects of the work in ensuring that questions related to the accuracy or integrity of any part of the work are appropriately investigated and resolved. All persons designated as authors qualify for authorship, and all those who qualify for authorship are listed. Data were collected with the ethics requirement that the participants' data are confidential and will not be shared. Any questions should be directed to the corresponding author.

DISCLOSURES

No conflicts of interest, financial or otherwise, are declared by the authors.

AUTHOR CONTRIBUTIONS

A.W., S.J., J.R.S., and J.M.M. conceived and designed research; A.W. and S.R. performed experiments; A.W. analyzed data; A.W. interpreted results of experiments; A.W. prepared figures; A.W. drafted manuscript; A.W., S.R., E.E., S.J., J.R.S., and J.M.M. edited and revised manuscript; A.W., S.R., E.E., S.J., J.R.S., and J.M.M. approved final version of manuscript.

REFERENCES

1. **Anderson DJ, Groves A, Lo L, Ma Q, Rao M, Shah NM, Sommer L.** Cell lineage determination and the control of neuronal identity in the neural crest. *Cold Spring Harb Symp Quant Biol* 62: 493–504, 1997. doi:10.1101/SQB.1997.062.01.056.
2. **Anderson RL, Jobling P, Gibbins IL.** Development of electrophysiological and morphological diversity in autonomic neurons. *J Neurophysiol* 86: 1237–1251, 2001. doi:10.1152/jn.2001.86.3.1237.
3. **Baldwin T.** Morality and human embryo research. Introduction to the talking point on morality and human embryo research. *EMBO Rep* 10: 299–300, 2009. doi:10.1038/embor.2009.37.
4. **Bharmal S, Slonimsky JD, Mead JN, Sampson CP, Tolkovsky AM, Yang B, Bargman R, Birren SJ.** Target cells promote the development

and functional maturation of neurons derived from a sympathetic precursor cell line. *Dev Neurosci* 23: 153–164, 2001. doi:10.1159/000048707.
5. **Bhatt S, Diaz R, Trainor PA.** Signals and switches in Mammalian neural crest cell differentiation. *Cold Spring Harb Perspect Biol* 5: a008326, 2013. doi:10.1101/cshperspect.a008326.
6. **Bradfield JS, Ajijola OA, Vaseghi M, Shivkumar K.** Mechanisms and management of refractory ventricular arrhythmias in the age of autonomic modulation. *Heart Rhythm* 15: 1252–1260, 2018. doi:10.1016/j.hrthm.2018.02.015.
7. **Brain KL, Trout SJ, Jackson VM, Dass N, Cunnane TC.** Nicotine induces calcium spikes in single nerve terminal varicosities: a role for intracellular calcium stores. *Neuroscience* 106: 395–403, 2001. doi:10.1016/S0306-4522(01)00280-9.
8. **Chambers SM, Fasano CA, Papapetrou EP, Tomishima M, Sadelain M, Studer L.** Highly efficient neural conversion of human ES and iPS cells by dual inhibition of SMAD signaling. *Nat Biotechnol* 27: 275–280, 2009. doi:10.1038/nbt.1529.
9. **Chambers SM, Mica Y, Studer L, Tomishima MJ.** Converting human pluripotent stem cells to neural tissue and neurons to model neurodegeneration. *Methods Mol Biol* 793: 87–97, 2011. doi:10.1007/978-1-61779-328-8_6.
10. **Chaudhuri KR.** Autonomic dysfunction in movement disorders. *Curr Opin Neurol* 14: 505–511, 2001. doi:10.1097/00019052-200108000-00012.
11. **Chung KF, Sicard F, Vukicevic V, Hermann A, Storch A, Huttner WB, Bornstein SR, Ehrhart-Bornstein M.** Isolation of neural crest derived chromaffin progenitors from adult adrenal medulla. *Stem Cells* 27: 2602–2613, 2009. doi:10.1002/stem.180.
12. **Collura CA, Johnson JN, Moir C, Ackerman MJ.** Left cardiac sympathetic denervation for the treatment of long QT syndrome and catecholaminergic polymorphic ventricular tachycardia using video-assisted thoracic surgery. *Heart Rhythm* 6: 752–759, 2009. doi:10.1016/j.hrthm.2009.03.024.
13. **Coskun V, Lombardo DM.** Studying the pathophysiologic connection between cardiovascular and nervous systems using stem cells. *J Neurosci Res* 94: 1499–1510, 2016. doi:10.1002/jnr.23924.
14. **Devay P, McGehee DS, Yu CR, Role LW.** Target-specific control of nicotinic receptor expression at developing interneuronal synapses in chick. *Nat Neurosci* 2: 528–534, 1999. doi:10.1038/9183.
15. **Franzoso M, Zaglia T, Mongillo M.** Putting together the clues of the everlasting neuro-cardiac liaison. *Biochim Biophys Acta* 1863, 7 Pt B: 1904–1915, 2016. doi:10.1016/j.bbamcr.2016.01.009.
16. **Ghasemi-Dehkordi P, Allahbakhshian-Farsani M, Abdian N, Mirzaeian A, Saffari-Chaleshtori J, Heybati F, Mardani G, Karimi-Taghanaki A, Doosti A, Jami M-S, Abolhasani M, Hashemzadeh-Chaleshtori M.** Comparison between the cultures of human induced pluripotent stem cells (hiPSCs) on feeder-and serum-free system (Matrigel matrix), MEF and HDF feeder cell lines. *J Cell Commun Signal* 9: 233–246, 2015. doi:10.1007/s12079-015-0289-3.
17. **Habecker BA, Anderson ME, Birren SJ, Fukuda K, Herring N, Hoover DB, Kanazawa H, Paterson DJ, Ripplinger CM.** Molecular and cellular neurocardiology: development, and cellular and molecular adaptations to heart disease. *J Physiol* 594: 3853–3875, 2016. doi:10.1113/JP271840.
18. **Herring N, Kalla M, Paterson DJ.** The autonomic nervous system and cardiac arrhythmias: current concepts and emerging therapies. *Nat Rev Cardiol* 16: 707–726, 2019. doi:10.1038/s41569-019-0221-2.
19. **Huguenard JR, Zbicz KL, Lewis DV, Evans GJ, Wilson WA.** The ionic mechanism of the slow outward current in Aplysia neurons. *J Neurophysiol* 54: 449–461, 1985. doi:10.1152/jn.1985.54.2.449.
20. **Itzhaki I, Maizels L, Huber I, Zwi-Dantsis L, Caspi O, Winterstern A, Feldman O, Gepstein A, Arbel G, Hammerman H, Boulos M, Gepstein L.** Modelling the long QT syndrome with induced pluripotent stem cells. *Nature* 471: 225–229, 2011. doi:10.1038/nature09747.
21. **Ji S, Tosaka T, Whitfield BH, Katchman AN, Kandil A, Knollmann BC, Ebert SN.** Differential rate responses to nicotine in rat heart: evidence for two classes of nicotinic receptors. *J Pharmacol Exp Ther* 301: 893–899, 2002. doi:10.1124/jpet.301.3.893.
22. **Jobling P, Gibbins IL.** Electrophysiological and morphological diversity of mouse sympathetic neurons. *J Neurophysiol* 82: 2747–2764, 1999. doi:10.1152/jn.1999.82.5.2747.
23. **Jobling P, McLachlan EM, Sah P.** Calcium induced calcium release is involved in the afterhyperpolarization in one class of guinea pig sympathetic neurone. *J Auton Nerv Syst* 42: 251–257, 1993. doi:10.1016/0165-1838(93)90370-A.
24. **Jonsson MK, Vos MA, Mirams GR, Duker G, Sartipy P, de Boer TP, van Veen TAB.** Application of human stem cell-derived cardiomyocytes in safety pharmacology requires caution beyond hERG. *J Mol Cell Cardiol* 52: 998–1008, 2012. doi:10.1016/j.yjmcc.2012.02.002.
25. **Kalla M, Herring N, Paterson DJ.** Cardiac sympatho-vagal balance and ventricular arrhythmia. *Auton Neurosci* 199: 29–37, 2016. doi:10.1016/j.autneu.2016.08.016.
26. **Killeen MJ, Sabir IN, Grace AA, Huang CL.** Dispersions of repolarization and ventricular arrhythmogenesis: lessons from animal models. *Prog Biophys Mol Biol* 98: 219–229, 2008. doi:10.1016/j.pbiomolbio.2008.10.008.
27. **Kimura K, Ieda M, Fukuda K.** Development, maturation, and transdifferentiation of cardiac sympathetic nerves. *Circ Res* 110: 325–336, 2012. doi:10.1161/CIRCRESAHA.111.257253.
28. **Larsen HE, Lefkimmiatis K, Paterson DJ.** Sympathetic neurons are a powerful driver of myocyte function in cardiovascular disease. *Sci Rep* 6: 38898, 2016. doi:10.1038/srep38898.
29. **Leong IUS, Skinner JR, Shelling AN, Love DR.** Zebrafish as a model for long QT syndrome: the evidence and the means of manipulating zebrafish gene expression. *Acta Physiol (Oxf)* 199: 257–276, 2010. doi:10.1111/j.1748-1716.2010.02111.x.
30. **Ludwig A, Zong X, Jeglitsch M, Hofmann F, Biel M.** A family of hyperpolarization-activated mammalian cation channels. *Nature* 393: 587–591, 1998. doi:10.1038/31255.
31. **Moretti A, Bellin M, Welling A, Jung CB, Lam JT, Bott-Flügel L, Dorn T, Goedel A, Höhnke C, Hofmann F, Seyfarth M, Sinnecker D, Schömig A, Laugwitz KL.** Patient-specific induced pluripotent stem-cell models for long-QT syndrome. *N Engl J Med* 363: 1397–1409, 2010. doi:10.1056/NEJMoa0908679.
32. **Oh Y, Cho G-S, Li Z, Hong I, Zhu R, Kim M-J, Kim YJ, Tampakakis E, Tung L, Huganir R, Dong X, Kwon C, Lee G.** Functional coupling with cardiac muscle promotes maturation of hPSC-derived sympathetic neurons. *Cell Stem Cell* 19: 95–106, 2016. doi:10.1016/j.stem.2016.05.002.
33. **Priori SG, Wilde AA, Horie M, Cho Y, Behr ER, Berul C, Blom N, Brugada J, Chiang C-E, Huikuri H, Kannankeril P, Krahn A, Leenhardt A, Moss A, Schwartz PJ, Shimizu W, Tomaselli G, Tracy C.** HRS/EHRA/APHRS expert consensus statement on the diagnosis and management of patients with inherited primary arrhythmia syndromes: document endorsed by HRS, EHRA, and APHRS in May 2013 and by ACCF, AHA, PACES, and AEPC in June 2013. *Heart Rhythm* 10: 1932–1963, 2013. doi:10.1016/j.hrthm.2013.05.014.
34. **Rajendran PS, Challis RC, Fowlkes CC, Hanna P, Tompkins JD, Jordan MC, Hiyari S, Gabris-Weber BA, Greenbaum A, Chan KY, Deverman BE, Münzberg H, Ardell JL, Salama G, Gradinaru V, Shivkumar K.** Identification of peripheral neural circuits that regulate heart rate using optogenetic and viral vector strategies. *Nat Commun* 10: 1944, 2019. doi:10.1038/s41467-019-09770-1.
35. **Ripplinger CM, Noujaim SF, Linz D.** The nervous heart. *Prog Biophys Mol Biol* 120: 199–209, 2016. doi:10.1016/j.pbiomolbio.2015.12.015.
36. **Rotthier A, Baets J, Timmerman V, Janssens K.** Mechanisms of disease in hereditary sensory and autonomic neuropathies. *Nat Rev Neurol* 8: 73–85, 2012. doi:10.1038/nrneurol.2011.227.
37. **Sargent PB.** The diversity of neuronal nicotinic acetylcholine receptors. *Annu Rev Neurosci* 16: 403–443, 1993. doi:10.1146/annurev.ne.16.030193.002155.
38. **Sharma A, Li G, Rajarajan K, Hamaguchi R, Burridge PW, Wu SM.** Derivation of highly purified cardiomyocytes from human induced pluripotent stem cells using small molecule-modulated differentiation and subsequent glucose starvation. *J Vis Exp* 18: 52628, 2015. doi:10.3791/52628.
39. **Shi Y, Kirwan P, Livesey FJ.** Directed differentiation of human pluripotent stem cells to cerebral cortex neurons and neural networks. *Nat Protoc* 7: 1836–1846, 2012. doi:10.1038/nprot.2012.116.
40. **Skinner JR, Winbo A, Abrams D, Vohra J, Wilde AA.** Channelopathies that lead to sudden cardiac death: clinical and genetic aspects. *Heart Lung Circ* 28: 22–30, 2019. doi:10.1016/j.hlc.2018.09.007.
41. **Takahashi K, Yamanaka S.** Induction of pluripotent stem cells from mouse embryonic and adult fibroblast cultures by defined factors. *Cell* 126: 663–676, 2006. doi:10.1016/j.cell.2006.07.024.
42. **Takayama Y, Kushige H, Akagi Y, Suzuki Y, Kumagai Y, Kida YS.** Selective induction of human autonomic neurons enables precise control

of cardiomyocyte beating. *Sci Rep* 10: 9464, 2020. doi:10.1038/s41598-020-66303-3.

43. **Thomson JA, Itskovitz-Eldor J, Shapiro SS, Waknitz MA, Swiergiel JJ, Marshall VS, Jones JM.** Embryonic stem cell lines derived from human blastocysts. *Science* 282: 1145–1147, 1998. doi:10.1126/science.282.5391.1145.
44. **Winbo A, Paterson DJ.** The brain-heart connection in sympathetically triggered inherited arrhythmia syndromes. *Heart Lung Circ* 29: 529–537, 2020. doi:10.1016/j.hlc.2019.11.002.
45. **Zaza A, Malfatto G, Schwartz PJ.** Sympathetic modulation of the relation between ventricular repolarization and cycle length. *Circ Res* 68: 1191–1203, 1991. doi:10.1161/01.RES.68.5.1191.